In Situ Microscopic Analysis of Asbestos and Synthetic Vitreous Fibers Retained in Hamster Lungs following Inhalation

Rick A. Rogers,[1] James M. Antonini,[1] Hjalmar Brismar,[1] Jean Lai,[1] Thomas W. Hesterberg,[2] Eben H. Oldmixon,[1] Philippe Thevenaz,[3] and Joseph D. Brain[1]

[1]Department of Environmental Health, Harvard School of Public Health, Boston, MA 02115 USA; [2]Johns Manville International, Denver, CO 80162 USA; [3]Research Consulting Company Ltd., Füllinsdorf, Switzerland

Hamsters breathed, nose-only, for 13 weeks, 5 days/week, 6 hr/day, either man-made vitreous fiber (MMVF)10a, MMVF33, or long amosite asbestos at approximately 300 World Health Organization (WHO) fibers/cc or long amosite at 25 WHO fibers/cc. [World Health Organization fibers are longer than 5 µm and thicker than 3 µm, with aspect ratio >3.] After sacrifice, fiber burden was estimated (left lungs) by ashing and scanning electron microscopy (ashing/SEM) or (right middle lobes) by confocal laser scanning microscopy (CLSM) *in situ*. *In situ* CLSM also provided three-dimensional views of fibers retained, undisturbed, in lung tissue. Fibers of each type were lodged in alveoli and small airways, especially at airway bifurcations, and were seen fully or partly engulfed by alveolar macrophages. Amosite fibers penetrated into and through alveolar septa. Length densities of fibers in parenchyma (total length of fiber per unit volume of lung) were estimated stereologically from fiber transsections counted on two-dimensional optical sections and were 30.5, 25.3, 20.0, and 81.6 mm/mm^3 for MMVF10a, MMVF33, and low- and high-dose amosite, respectively. Lengths of individual fibers were measured in three dimensions by tracking individual fibers through series of optical sections. Length distributions of amosite fibers aerosolized, but before inhalation versus after retention in the lung were similar, whether determined by ashing/SEM or *in situ* CLSM. In contrast, the fraction of short MMVF10a and MMVF33 fibers increased and the geometric mean fiber lengths of both MMVFs decreased by approximately 60% during retention. Most likely due to fiber deposition pattern and differences in sampling, fiber burdens [MMVF10a, MMVF33, and amosite (high dose; 269 WHO fibers/cc)] determined by ashing/SEM were 1.4, 1.5, and 3.5 times greater, respectively, than those calculated from *in situ* CLSM data. *In situ* CLSM is able to provide detailed information about the anatomic sites of fiber retention and also fiber lengths and burdens in good agreement with ashing/SEM results. *Key words*: aerosol, amosite asbestos, ashing, confocal microscopy, fiber burden, man-made fibers, MMVF, respirable, three-dimensional. *Environ Health Perspect* 107:367–375 (1999). [Online 26 March 1999] *http://ehpnet1.niehs.nih.gov/docs/1999/107p367-375rogers/abstract.html*

The health effects of exposure to airborne asbestos and synthetic fibers have been extensively studied, as reviewed by DeVuyst et al. (*1*) and Hesterberg et al. (*2*). The respiratory system's response to fibers depends greatly on fiber composition, fiber length, the sites of deposition, the tissue compartments through which fibers move, and the rates at which they are cleared (*3,4*). Such health effects also depend on the amount of fiber deposition in the respiratory system and the resulting fiber burden. This has traditionally been determined by recovering fibers from lungs using thermal ashing techniques or chemical digestion by strong bases and oxidizing agents (*5–7*). Despite a considerable body of work, little is known about either the distribution of artificial fibers within the lungs after exposure or the local responses of lungs to fiber deposition. Indeed, it has been difficult to obtain such information because, although digestion methods permit determinations of numbers and dimensions of all fibers retained in the lung, neither fiber position within pulmonary structures nor any relationship to regional lung pathology can be recovered. Also, visualization methods available hitherto have required that the lung be finely sectioned physically to examine the fibers directly.

The mechanical properties of the fibers themselves make them difficult to approach without disturbing or breaking them; not only are they needlelike (inhaled fibers frequently have aspect ratios >5:1 and may be over 20 µm in length), they also may be both rigid and fragile. Thus, if samples of lung tissue are embedded in paraffin and physically sectioned in preparation for conventional transmission light microscopy, the fibers may be cut, disturbed, or torn out of the section during the cutting process, as fibers would typically not lie entirely within physical sections that may be 6–8 µm in thickness. Transmission electron microscopy (TEM) has been used to image fibers within fixed lung tissue (*8,9*), but here, especially, the process of obtaining physical sections for TEM (60–70 nm thick) can be expected to cut apart every fiber encountered and to introduce artifacts (*6*). Scanning electron microscopy (SEM) permits intact fibers to be studied, especially following freeze-etching or dissection along bronchi; however, SEM images show primarily the surfaces of fibers, cells, and tissue that are closest to the observer.

Confocal microscopy, however, makes it possible to peer tens or hundreds of microns below the surface of a translucent specimen and recover two-dimensional images from essentially any location within it, even revealing fibers within cells or tissues. Data volumes (three spatial dimensions plus intensity values) built up from such two-dimensional images obtained from increasing depths can be presented as stereoscopic (quasi-three-dimensional) pictures showing, for example, intact, undisturbed fibers penetrating alveolar walls.

The present study's purpose was to determine the numbers and locations of three types of fibers [two man-made vitreous fibers (MMVFs) and long amosite asbestos, a naturally occurring mineral fiber] that had been inhaled into hamster lungs. We utilized confocal microscopy to examine relatively large embedded lung tissue samples with minimal disruption of the fibers deposited there and compared the results to those obtained by SEM of ashing residue.

Materials and Methods

Experimental Design

This article presents results obtained by examining material produced as part of a larger study. The parent study was an 83-week chronic inhalation study with interim sacrifices; the first one, after 13 weeks of exposure, supplied the material for the present investigation. There were 125 hamsters in each of five exposure groups and 140 in

Address correspondence to R.A. Rogers, Department of Environmental Health, Building I, Room 1315, Harvard School of Public Health, 665 Huntington Avenue, Boston, MA 02115 USA.

We express our thanks for the expert technical support of Bruce A. Ekstein, Emily Sullivan, Kafi Meadows, Jenny Roberts, Michael Roberts, and Karl Mink for assistance in quantitative confocal microscopic analysis. We also wish to thank William C. Müller of Johns Manville Technical Center for providing ashing/SEM data. This work was supported by HL453510, HL33009, the North American Insulation Manufacturers Association, NIEHS-ES00002, and NIOSH-109979.

Received 13 October 1998; accepted 14 January 1999.

an air control group. Some results from the parent study have been published (*10*).

Experimental Material

Fibers. Three types of fibers were studied: 1) MMVF10a, a glass fiber commonly used in building insulation; 2) MMVF33, a glass fiber used in the manufacture of high-efficiency air-purification filter systems; and 3) long amosite, a form of naturally occurring mineral asbestos. World Health Organization (WHO) fibers have aspect ratio >3, length >5 μm, and diameter <3 μm (*11*).

Animals. Male Syrian golden hamsters (strain LakCrl:LVG) of specific-pathogen-free quality were housed and exposed to aerosolized fiber at Research Consulting Co. (Füllinsdorf, Switzerland). They were housed individually in Makrolon type-I cages (EHRET GmbH, Emmendingen, Germany) containing dust-free, softwood bedding (Lignocel, Schill AG, Muttenz, Switzerland) in a specific-pathogen-free environment. Pelleted food and water were provided *ad libitum*. This breed has been used in previous inhalation studies with natural and/or synthetic vitreous fibers (*12*).

Experimental Exposure

Animals were divided into six groups (five exposure groups and one air control group). Group 1 (MMVF10a fibers) was composed of animals exposed to 339 WHO fibers/cc (29.6 mg/mm^3); group 2 (MMVF33 fibers) was composed of animals exposed to 310 WHO fibers/cc (37.0 mg/mm^3); group 3 (long amosite, low concentration) animals received 36 WHO fibers/cc (0.8 mg/mm^3); group 4 (long amosite, medium concentration) animals received 165 WHO fibers/cc (3.7 mg/mm^3); group 5 (long amosite, high concentration) animals were exposed to 269 WHO fibers/cc (7.1 mg/mm^3); and group 6 (air control) animals received no fibers, only air. For nose-only exposure to aerosols or filtered air, all animals were placed in restraint tubes for 6 hr/day, 5 days/week for 13 weeks; during the rest of the time, they breathed clean filtered room air. One day after the exposure period, hamsters were anesthetized with an intraperitoneal injection of sodium pentobarbital (300 mg/kg body weight) and sacrificed by exsanguination, whereupon their lungs were excised.

Specimen Preparation for *in Situ* Microscopic Examination

Fixation and embedment. The middle lobe of the right lung of each hamster was processed for microscopic examination of fibers *in situ*. The right lung was detached between lung and hilum, fixed by instilling 4% buffered paraformaldehyde into the airways at 30 cm water pressure, then shipped from Switzerland to Boston. The lung samples remained in the fixative for up to 10 days. Each right middle lobe was cut sagitally into five pieces 5 mm thick, dehydrated in graded ethanolic series to absolute ethanol, stained nonspecifically with the fluorescent dye lucifer yellow CH [0.001% w/v in absolute ethanol; (*13*)], and embedded in Spurr's epoxy (Polysciences, Warrington, PA). The results of Law et al. (*14*) suggest that at most 16% of the silica content of the most susceptible MMVFs would be dissolved in this time, and that the loss could be less than 1% from all fiber types.

Sample manipulation. Epoxy-embedded samples were attached to a metal adapter plate and mounted on a high-speed milling apparatus, where the top of the block was milled to a glassy smoothness (*15*). The sample on its adapter plate was then attached to a stage with digital readouts on the confocal laser scanning microscope/microscopy (CLSM). The CLSM can only retrieve optical sections to a certain depth, the depth limit depending on objective working length and the severity of light scattering and absorption by the sample. Material below this depth limit could be imaged by returning the sample block to the milling apparatus to remove some of the already imaged overlying tissue. Upon its return to the CLSM, the block could be positioned in three dimensions to within 1 μm of its previous position.

Specimen Preparation for Ash Analysis

The left lung (detached between lung and hilum) was frozen at autopsy and shipped frozen from Switzerland to the Johns Manville International, Inc., analysis laboratories (Littleton, CO). To recover inhaled fibers from the lung for these evaluations, tissue from the left lung was subjected to a low-temperature ashing process as previously described (*7,10,16*); the ash residue was suspended in deionized filtered water, sonicated, and filtered onto a polycarbonate membrane filter (Nucleopore; Bio-Rad Laboratories, Hercules, CA; 0.2 μm pore size), which was mounted on a specimen planchet, coated with gold, and examined by SEM. Fibers were counted and measured according to methods described previously (*10*).

Imaging of Fibers and Lung Tissue by CLSM

CLSM configuration. The CLSM was a Sarastro 2000 (Molecular Dynamics, Sunnyvale, CA) fitted with a 25-mW argon ion laser providing 488 nm wavelength excitation illumination. Either 20× (NA 0.8) or 60× (NA 1.4) objectives were used; a polarizing filter placed in the emitted light's path transmitted properly polarized light reflected from fibers.

The CLSM was configured with two channels, each with a separate photomultiplier detector. In channel 1, used for fluorescence (tissue) detection, light (wavelengths >510 nm) emitted from dye-stained tissue was directed to detector 1. In channel 2, used for reflected light (fiber) detection, illuminating light reflected from fibers (wavelengths <510 nm) passed through a 510-nm secondary beam splitter and was directed to detector 2.

Each field-of-view (FOV), therefore, was represented by two digital images—one from each channel—and such pairs of images could be superimposed to show fiber positions in relation to lung tissue. Optical sections lay in the microscope's (x,y) focal plane.

Fiber samples: imaging by CLSM. Samples of dry stock MMVF10a, MMVF33, and long amosite asbestos fibers were obtained from the NAIMA (North American Insulation Manufacturers Association, Alexandria, VA) fiber repository and were suspended (1 mg/ml) in saline and allowed to settle in microwell chambers for CLSM. Micrographs of fibers were obtained with the CLSM configured as described previously, using the 20× and 60× objectives.

Lung tissue and fibers retained in lung: imaging by CLSM. The CLSM was used to look through the smooth surfaces of the epoxy-embedded tissue samples to as much as 150 μm below the surface without physically sectioning the samples.

Stacks of aligned optical sections were acquired between two depths sufficiently separated to completely contain essentially all fibers detected within them. This technique permitted us to determine the length densities, length distributions, and anatomic placement of retained long amosite and MMVF fibers in lungs. Three-dimensional projections were generated from stacks of optical sections using Voxel View software (Vital Images, Inc., Fairfield IA) (*17*).

CLSM images for stereologic length densities. Length density refers to the length of a linear structure present within a unit volume of some containing phase; here, it refers to the total length of retained fiber per unit volume of lung and has units such as millimeters per cubic millimeter. Micrographs were obtained with the CLSM configured as described previously, using the 20× objective. Each digital micrograph was a two-dimensional, 1,024 × 1,024 array

520.0 µm on a side of gray-scale pixels (intensity values from 0 to 255), 0.5078 µm on a side; thus, pixel area was 0.2579 μm^2 and image area 270,399 μm^2. FOVs were acquired at random locations over the tissue exposed at the prepared block face.

CLSM images for three-dimensional lengths of individual fibers. Each image, acquired with the 60× objective, was a 512 × 512 array 87 µm on a side of gray-scale pixels, 0.34 µm on a side. The images were obtained with a vertical spacing of 0.7 µm. Stacks encompassing >75 µm along the *z*-axis were obtained from locations where fibers were relatively plentiful.

Image segmentation to emphasize fibers in the presence of tissue. Prior to analysis, each pixel in the field of view was assigned to one of three categories: tissue, fiber, or other. This was done by setting pixels representing air and noise in the channel 1 (tissue) image to 0, leaving tissue pixels with values >0. Fiber pixels in channel 1 were 0-valued. The channel 2 (fiber) image was similarly thresholded, leaving >0 values in pixels representing fiber; because of the slight reflectivity of the tissue and weak fluorescent emissions occurring at short wavelengths, some tissue appeared faintly in channel 2. Pixels representing fibers could be distinguished as those that were 0 in channel 1 but of at least moderate intensity in channel 2; side-by-side comparisons of the channel 1 and 2 images made it easy to identify fiber profiles in the channel 2 image.

Length Densities of Fibers within the Lung, by *in Situ* CLSM

Fiber length densities (total length of retained fiber per unit volume of lung) were measured in four, five, five, and five animals from the MMVF10a, MMVF33, low-dose amosite, and high-dose amosite treatment groups, respectively (13-week exposure; no recovery period). Images were taken predominantly of the two tissue samples with large cut surfaces on both sides and were collected at random (regular grid with randomly positioned origin); exception to this random procedure was made in that FOVs with visible pleura or extrapulmonary space were not recorded. Fiber transsections visible on each image were counted manually.

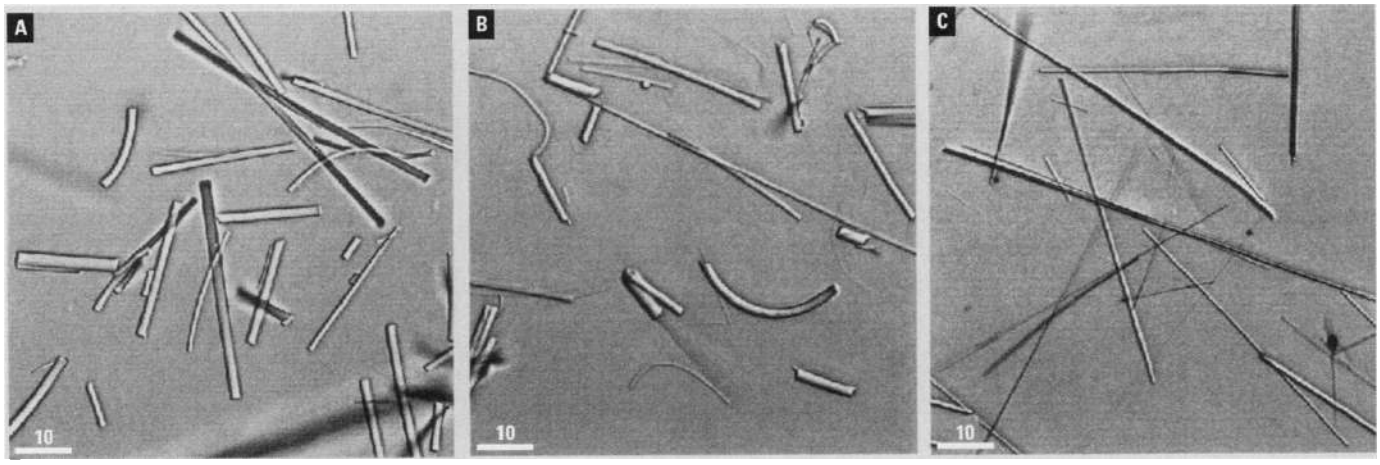

Figure 1. Three types of fibers before aerosolization imaged by confocal laser scanning microscopy operated in reflected light mode. Individual fibers of all types appear to be of constant diameter. (A) Man-made vitreous fiber (MMVF)10a: fibers appear somewhat narrower and more curved than MMVF33. (B) MMVF33: note aggregates of individually straight fibers. (C) Long amosite: straight fibers, apparently little aggregated. Bars represent 10 µm.

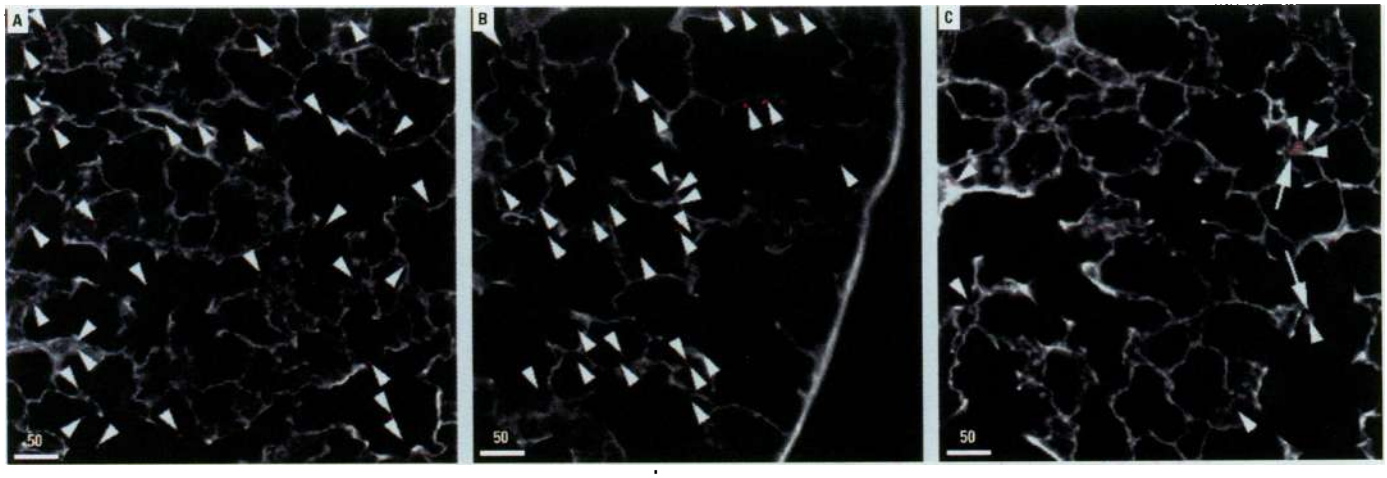

Figure 2. Hamster lungs after 13-week exposure to three fiber types. Optical sections acquired approximately 50 µm below cut surface of embedded tissue using confocal laser scanning microscopy operated in dual detector mode (reflected light for fibers, represented by red in figure; fluorescence for tissue, represented by grayscale in figure). At least 500 µm of epoxy with embedded tissue was milled away from the surface (see text) prior to examination to ensure that fibers seen here could not have been disturbed by the act of cutting samples from the fixed lung before embedment. (A) Man-made vitreous fiber (MMVF)10a: 31 fiber transsections seen in alveolar parenchyma; 21 are >5 µm from nearest septal profile. (B) MMVF33: 31 transsections of fibers (arrowheads) are seen within alveolar parenchyma; of these, 21 are more than approximately 5 µm from the nearest alveolar septal profile. Lung pleura is visible. (C) Long amosite: seven fiber transsections (arrowheads) and two alveolar macrophages (arrows) can be seen; one of the macrophages contains at least three fibers, the other, at least one. Bars represent 50 µm.

We assume that fibers retained in lung are randomly oriented with respect to the optical plane of section. The total length of linear features of interest (fibers) contained within a phase (lung) may be estimated (*18*) by

$$L_V = 2 \times \left(\frac{\sum_{i=1}^{n} Q_{F(i)}}{\sum_{i=1}^{n} A_{lung(i)}} \right) \quad (1)$$

where L_V is the length density of fibers in lung, i.e., length of fibers per unit volume lung; $Q_{F(i)}$ is the number of fiber transsections seen on image i; and $A_{lung(i)}$ is the transsected area of lung seen on image i (here, always equal to the area of an image [(*18*), Eq. 4.54a]).

Fiber Dimensions

Fiber dimensions before aerosolization, as determined by SEM. Lengths and diameters (analyzed using SEM and reported as mean, standard deviation, minimum, maximum, and median) of fibers to be aerosolized were obtained from NAIMA.

Dimensions of retained fibers, as determined by ashing/SEM. Numbers and dimensions of fibers after aerosolization, inhalation, retention, and ashing of the left lung were determined by analysis of SEM micrographs of fiber samples collected on Nucleopore polycarbonate filters (0.2 µm pore size) (*19*).

Fiber lengths as determined by CLSM in situ. The lengths of fibers retained in animals' right lungs were determined from fibers contained in stacks of optical sections. The length of a fiber was estimated as the sum of Pythagorean distances between transsections on successive optical sections, whose locations were marked in three dimensions (pixel located at coordinates x,y on section at depth z).

Fiber Burden

Fiber burden calculated from CLSM data. The number of fibers in parenchyma per lung was estimated by combining estimates of fiber length density and geometric mean fiber length with an assumed lung volume. (Lung volume was not measured directly.)

$$FB = \frac{L_V \times V_L}{\bar{\lambda}_{fiber}} \quad (2)$$

where FB is the fiber burden, number of fibers per left and right lung pair; L_V is the length density of fibers in lung, from two-dimensional CLSM data and stereology; V_L is the volume of lung, assumed to be 4.0 ml; $\bar{\lambda}_{fiber}$ is estimated geometric mean length of fibers, from three-dimensional CLSM data.

Results

Characteristics of Fibers before Aerosolization

Nonaerosolized samples of the three fiber types were examined by reflected light confocal microscopy. In Figure 1A (MMVF10a), the diameters along any given fiber appeared constant, but the fibers themselves occasionally were curved. Fibers occurred with a range of diameters, however. In Figure 1B (MMVF33), individual fibers appeared straight, often aggregated side to side and jumbled together. In Figure 1C (amosite), fibers appeared as straight rods of constant diameter, rarely clustered. All fiber types displayed brightnesses that varied depending on fiber orientation relative to the imaging plane, and they revealed interference patterns characteristic of fibers illuminated by polarized light. Practically the full lengths of the fibers were seen in these images, despite the optical sectioning property of confocal microscopy, because the fibers lay on a flat surface parallel to the optical sectioning plane. Because all fibers seen were in focus simultaneously, they must have been coplanar, and there was no indication of out-of-plane unobserved fibers. Hence, it is most likely that all fibers were clearly imaged and observed.

Placement of Retained Fibers

Samples of hamster lung following 13-week inhalation exposure to the three fiber types were examined using combined fluorescence and reflected light confocal microscopy. Fibers of each type reached the alveolar parenchyma and in some instances were taken up by alveolar macrophages (Fig. 2). Both MMVF10a (Fig. 2A) and MMVF33 (Fig. 2B) appeared throughout alveolar parenchyma, even occurring in subpleural regions. Fiber transsections often were seen some tens of microns away from the nearest septal profile, meaning that the fiber did not lie against an alveolar septum for its entire length but crossed an alveolar airspace. With

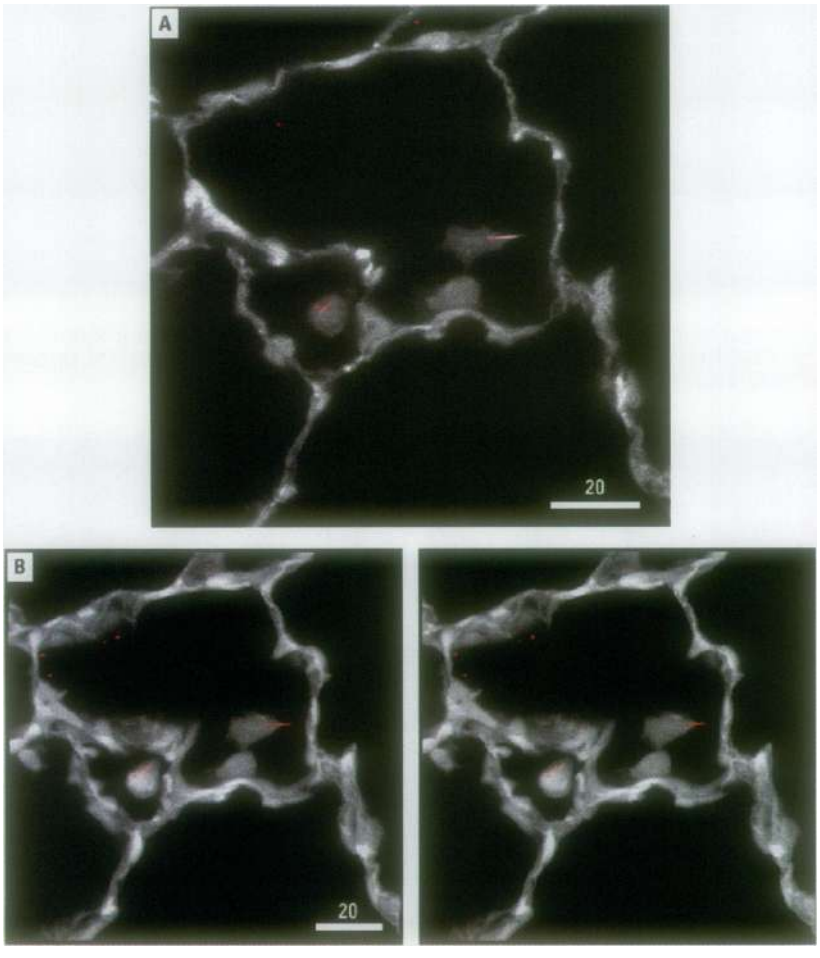

Figure 3. Man-made vitreous fiber (MMVF)10a fibers retained for up to 13 weeks in hamster lung, visualized by confocal laser scanning microscopy. Bars in (A) and (B) represent 20 µm. (A) A single optical section from a stack of serial optical sections obtained at 1-µm intervals. Inflammatory cells with partially or wholly ingested fibers (in red) are in the airspace. (B) Left and right panels: stereo projection of the entire stack. Fibers are visible both in inflammatory cells and free in airspace.

high-dose amosite (Fig. 2C), some fibers were found within alveolar macrophages (arrow, Fig. 2C).

Fibers of each type had reached alveolar parenchyma. Fiber placement within parenchyma was further established by examining stereoscopic views of stacked, aligned optical sections. For MMVF10a (Fig. 3A, 3B), fibers were present both free in the airspace and partially or wholly ingested by inflammatory cells. For MMVF33 (Fig. 4A, 4B), as with MMVF10a, some fibers were engulfed by inflammatory cells within alveolar air spaces (Fig. 4A, hollow arrow). A long fiber lay within the interstitium of an alveolar septum (Fig. 4A, arrow). The accompanying stereo projection (Fig. 4B) shows fiber position and orientation in alveoli. In amosite (Fig. 5A, 5B), a fiber (Fig. 5A, arrow) appears within the interstitial space adjacent to an airway. The stereo projection (Fig. 5B) shows this fiber to be entering the interstitium at an airway bifurcation (Fig. 5B, arrow). Numerous inflammatory cells containing fibers are present in the airway.

An alveolar macrophage can be seen attempting to engulf a long amosite fiber in Figure 6, which was acquired at higher magnification than Figures 3, 4, and 5. Most of the amosite fiber's length is either embedded in septal tissue or surrounded by the macrophage's cell body or its slender tapering processes.

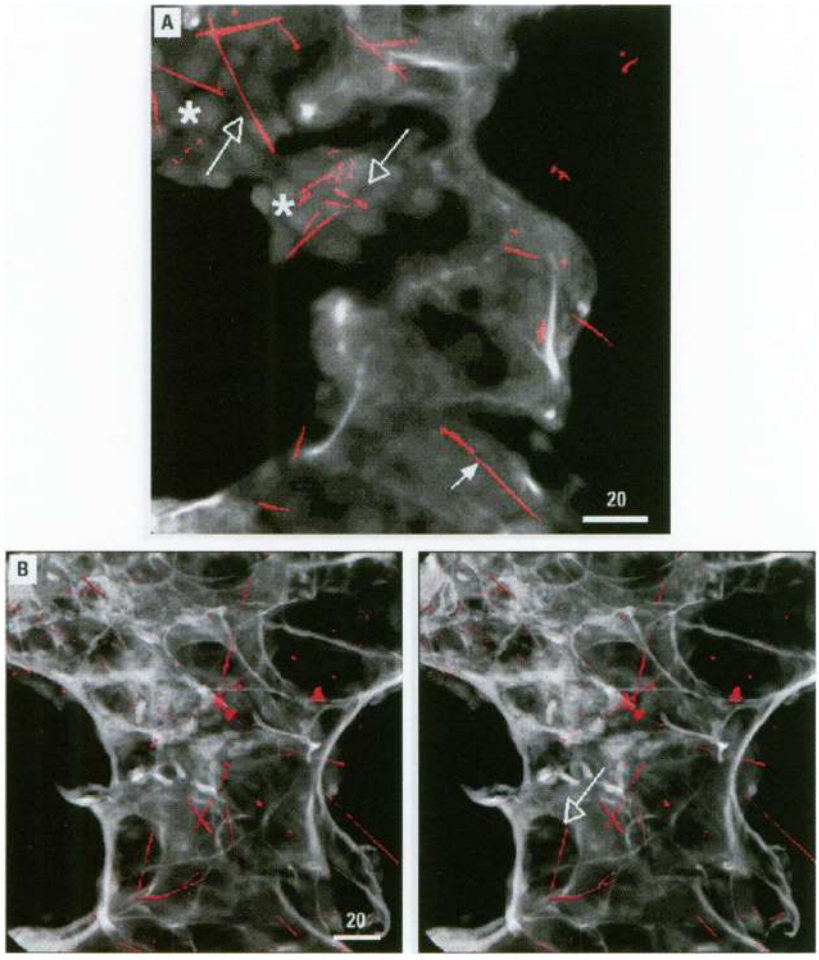

Figure 4. Man-made vitreous fiber (MMVF)33 fibers retained for up to 13 weeks in hamster lung, visualized by confocal laser scanning microscopy. Bars in (A) and (B) represent 20 µm. (A) A single representative optical section from a stack of 240 serial optical sections obtained at 1-µm intervals. Numerous inflammatory cells (asterisks) containing fibers (hollow arrows) are present in the airspace. In this optical section, fibers seemingly superimposed on tissue in reality lie within tissue, and thus a large fiber (solid arrow) lies within the interstitial space of an alveolar septum. (B) Left and right panels: stereo projection of the entire 240-section stack shows fiber position and orientation in representative alveolar parenchyma. The section shown in (A) comes from the part of this stack distant from the viewer. Collagen and elastin bundles, which appear in pale gray, reinforce and support airway bifurcations and alveolar entrance rings. Fibers are seen throughout alveolar parenchymal tissue and airspace (hollow arrow).

Length Distributions of Fibers as Aerosolized and after up to Thirteen Weeks of Retention

Table 1 summarizes lengths of MMVF10a, MMVF33, and long amosite asbestos fibers as measured in air and lung samples 1) present in the aerosol presented to the animal's nose; 2) after 13 weeks of exposure, by the ashing/SEM technique; and 3) after 13 weeks of exposure by *in situ* CLSM.

The order of aerosolized fiber lengths from longest to shortest (for both geometric mean lengths and median lengths) was MMVF10a, MMVF33, amosite; for retained fibers, the order was different—amosite, MMVF10a, MMVF33. Both MMVF types were shortened by approximately 60% (geometric mean). The geometric mean for amosite increased by 44%, whereas the arithmetic mean and median decreased by 9 and 6%, respectively. All fiber length distributions are skewed toward longer lengths (see below).

Figure 7 compares fiber length cumulative frequency distributions (FLCFDs) 1) for fibers in the aerosol, determined using SEM; 2) for retained fibers, using ashing/SEM; and 3) for retained fibers, using *in situ* CLSM. With MMVF10a (Fig. 7A), both analyses of retained fibers yielded similar FLCFDs and both found fewer long fibers than did aerosol analysis; in particular, 37% of fibers in the aerosol were longer than 20 µm while barely 5% of retained fibers were. With MMVF33 (Fig. 7B), ashing/SEM and *in situ* CLSM did not yield similar FLCFDs for retained fibers; the former showed a smaller proportion of short (<5 µm) fibers than did the latter. Both, however, showed fewer long fibers (>15 µm) than did aerosol analysis. With amosite asbestos (Fig. 7C), ashing/SEM analysis of retained fibers showed more short (<5 µm) and fewer long (>20 µm) fibers than did *in situ* CLSM. Neither analysis of retained fibers, however, showed as many long fibers as did aerosol analysis.

Figure 8 shows the complete FLCFD obtained by *in situ* CLSM for retained fibers of each type. The fraction of total fiber number lying between any two lengths may be read directly from Figure 8. For example, the proportion of fibers categorizable as respirable according to WHO standards (identical with the category of all fibers longer than 5.0 µm and listed in Table 2) may be obtained as the fraction of the ordinate above the crossing point of the FLCFD and the vertical dotted line at 5.0 µm. Similarly, these curves demonstrate that the proportion of long (>20 µm) fibers was less than 5% for MMVF10a, nearly 15% for MMVF33, and 25% for amosite.

Length Densities of Fibers in Lung by *in Situ* CLSM

Table 3 gives the number of FOVs examined, the number of fiber transsections found, and the calculated length density (Eq. 1) for each fiber treatment group. MMVF10a and MMVF33 apparently

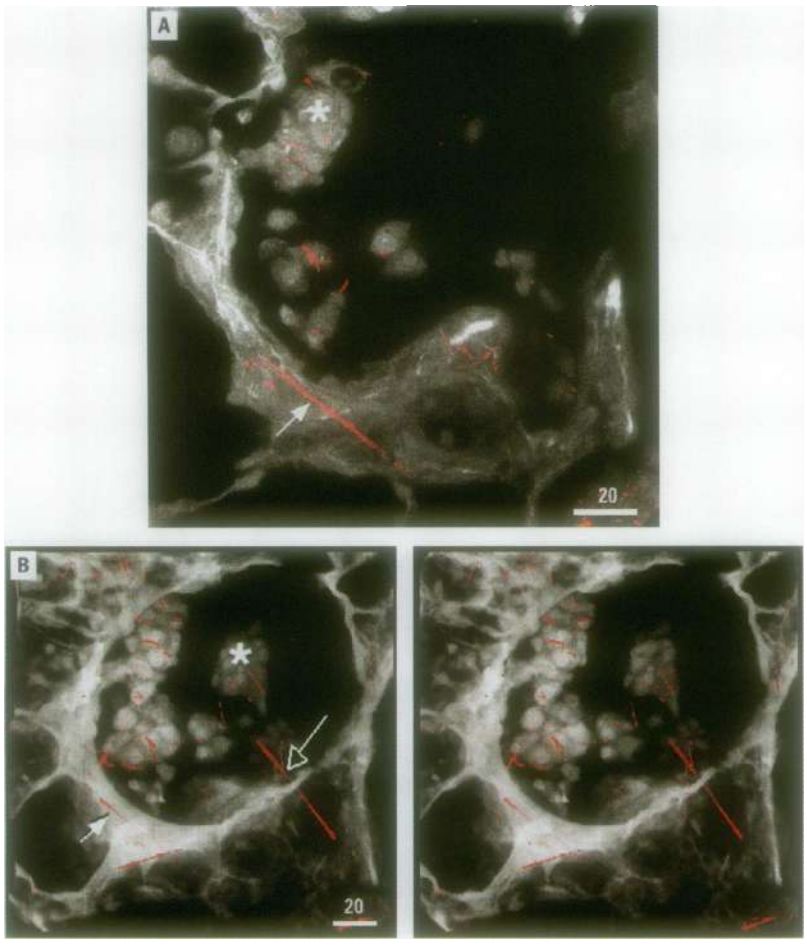

Figure 5. Long amosite fibers retained for up to 13 weeks in hamster lung. Optical sections acquired as for Figure 3. Bars in (A) and (B) represent 20 µm. (A) Single optical section selected from stack. A fiber (arrow) is seen within the interstitial space adjacent to an airway that contains inflammatory cells (asterisk). (B) Left and right panels: stereo projection of stack. The solid arrow points to the same fiber as in (A). It is seen to be located at an airway bifurcation. The numerous inflammatory cells present in the airway (e.g., asterisk) contain many short and long fibers. Note the presence of long straight fiber in both airway and alveolar airspace (hollow arrow); by examining the individual sections and viewing the reconstruction from different angles, this fiber can be seen to penetrate the tissue bounding the alveolar duct.

behaved similarly during retention, according to their distributions (given previously) and Table 3 demonstrates that length densities of these fibers were also comparable.

Fiber Burden

Fiber burdens (Eq. 2) of MMVF10a, MMVF33, and amosite (high dose) at the end of the 13-week exposure were estimated by two different techniques (ashing/SEM and *in situ* CLSM). Results are presented in Table 2, which lists the fraction of total fiber number in each 5-µm-wide length class up to 20 µm and the >20 µm length class; these numbers are the same as plotted in Figure 6 and were used to calculate the corresponding fiber burdens. The ratios between the fiber burdens for the two techniques are also provided for each fiber type. Discrepancies between the burdens are greatest for amosite. The burdens for amosite were two- to nine-fold greater with SEM than with CLSM, with the short fiber category (<5 µm long) showing the greatest disparity; in millions of fibers/lung, the burdens were 17 by SEM as compared to <2 by CLSM (Table 2). The two methods yielded fairly similar burdens for the two MMVFs, with SEM burden no more than 2.4-fold greater than CLSM. The distribution of the fiber burden by length class was similar for both MMVFs, except that MMVF33 had a greater number of long (>20 µm) fibers than did MMVF10a.

Discussion

Locations of Fibers Retained in Lung, by *in Situ* CLSM

We observed the placement of MMVF and asbestos fibers *in situ* in lung tissue after 13 weeks of exposure. Fibers of all three types

Table 1. Fiber lengths before and after retention in lung

Fiber type, experimental condition	Number of fibers measured	Arithmetic mean (SD) (µm)	Geometric mean (SD) (µm)	Mean (µm)	Range (µm)
MMVF10a					
Aerosolized (at nose, SEM)[a]	–	19.4 (20.9)	12.4 (0.916)	12.3	–
Postretention (ashing/SEM)[a]	–	7.98 (6.18)	6.4 (1.9)	6.12	–
Postretention (*in situ* CLSM)	256	6.95 (6.20)	5.15 (0.765)	4.66	0.98–59.0
Percent decrease	–	64.2	58.5	68.8	–
MMVF33					
Aerosolized (at nose, SEM)[a]	–	16.9 (16.3)	11.8 (0.832)	11.9	–
Postretention (ashing/SEM)[a]	–	9.97 (8.38)	7.6 (2.1)	7.15	–
Postretention (*in situ* CLSM)	250	9.40 (14.1)	4.77 (1.12)	3.50	0.51–74.8
Percent decrease	–	44.4	59.6	67.3	–
Long amosite					
Aerosolized (at nose, SEM)[a]	–	18.4 (16.7)	8.6 (0.875)	7.8	–
Postretention (ashing/SEM)[a]	–	11.68 (9.68)	8.4 (2.1)	8.88	–
Postretention (*in situ* CLSM)	396	16.8 (15.2)	12.4 (0.775)	12.08	2.67–113
Percent decrease	–	8.7	-44.2	6.4	–

Abbreviations: SD, standard deviation; MMVF, man-made vitreous fiber; SEM, scanning electron microscopy; CLSM, confocal laser scanning microscopy. Descriptive statistics for lengths of three types of fibers (MMVF10a, MMVF33, and amosite asbestos) as present in aerosol administered to hamsters and from hamster lungs after 13 weeks of exposure, as determined by ashing/SEM or *in situ* CLSM.

[a]Results from Miller (*19*).

were deposited in small airways and alveolar septa, frequently being seen at airway bifurcations; this agrees with observations of Brody et al. (*8*) and Brody and Roe (*20*). Long amosite asbestos fibers frequently penetrated into alveolar septa as far as the interstitium and even completely through septa, in accord with the demonstrated ability of fibers to penetrate lung tissue (*21–23*). MMVF fibers were not observed to penetrate septa as frequently as did amosite fibers, however. Fibers of all types were found within alveolar macrophages.

Effects of Length-biased Filtering during Respiration and Fiber Fragmentation and Degradation during Retention

As in previous rodent inhalation studies (*24*), the present study demonstrated that both arithmetic and geometric mean lengths of MMVF fibers in aerosol were typically longer than those of retained fibers. This difference could be the result of a lung filtering process in which longer fibers are prevented from being inhaled into the distal alveolar parenchymal portions of the lung, or it could be a result of fiber degradation within the lung, or both.

In the case of amosite (Fig. 7C), the aerosol FLCFD and retained FLCFD obtained by *in situ* CLSM were similar, suggesting that amosite fibers of all lengths were equally likely to reach parenchyma—that is, that no significant filtering process affected amosite fibers. Because the FLCFD of retained amosite fibers was obtained after 13 weeks of exposure—adequate time for fiber fragmentation and degradation to have occurred in the lung—it seems that amosite fibers also resisted breakage and degradation and remained intact.

MMVF10a and MMVF33, on the other hand, showed strong reductions in arithmetic and geometric mean lengths (Table 1) and a strong increase (Fig. 7A, 7B) in the proportion of short fibers over the same time period. The 13-week time point cannot shed much light on which process (filtration or degradation) is more important in causing these changes because the possible filtration effects could be masked by effects of degradation. However, as part of the chronic study, fiber lengths were determined after only 6 hr of retention (*10,19*), and the proportion of long fibers by fiber type was as follows: MMVF10a: aerosol>6 hr>13 weeks, suggesting that both lung filtration and fiber degradation were contributing factors; MMVF33: aerosol>6 hr = 13 weeks, suggesting filtration but not degradation; amosite: aerosol = 6 hr = 13 weeks, suggesting neither filtration nor degradation. The absence of a filtration effect on amosite fibers might be due to the narrower fiber diameters of that mineral as compared to the MMVFs, which could give long amosite fibers a smaller, hence more respirable, aerodynamic diameter than long MMVF fibers, which might have an aerodynamic diameter large enough to make them less respirable.

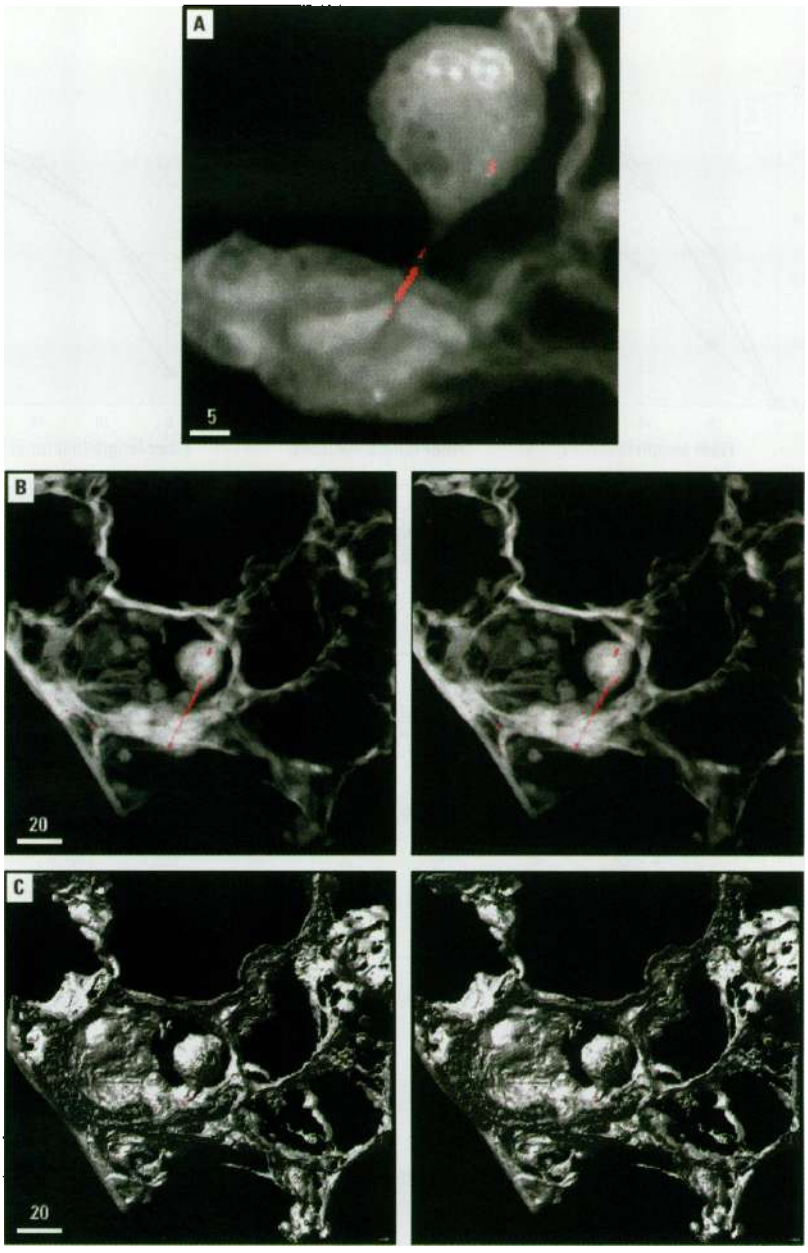

Figure 6. Close-up examination of an amosite fiber partially implanted in interstitium and partially engulfed by an alveolar macrophage. (A) An optical section 1.3-µm thick selected from a stack of sections 100-µm thick shows an amosite fiber (red) passing from septum through alveolar airspace and into an alveolar macrophage. Bar represents 5 µm. (B) Left and right panels: stereoscopic look-through projection of the entire stack, in which tissue appears translucent. Fiber is visible not only in airspace, but also within both septum and macrophage. Bar represents 20 µm. (C) Left and right panels: stereoscopic reconstruction of tissue and fiber surfaces; the entire stack has been rendered as though the tissue were opaque and slightly reflective. Only a few microns of the fiber's length are not covered by septal tissue or the macrophage, showing that the fiber indeed was embedded within these structures. Bar represents 20 µm.

Comparison of Two Methods for Measuring Lung Fiber Burden

The literature suggests that destroying the lung to assay retained fibers may change their lengths; Warheit et al. (*6*) showed that glass fiber dimensions become modified during simulated tissue digestion, possibly leading to an overestimation of the numbers of fibers/lung (e.g., as a result of

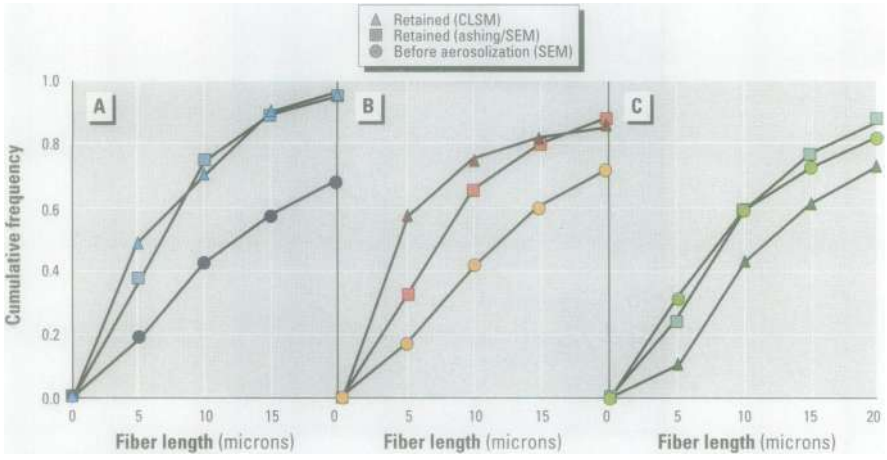

Figure 7. Five points on each fiber length cumulative frequency distribution for each fiber type before aerosolization and as retained in lung after 13-week exposure (ashing/SEM, CLSM). (A) MMVF10a; (B) MMVF33; and (C) amosite. Abbreviations: CLSM, confocal laser scanning microscopy; SEM, scanning electron microscopy; MMVF, man-made vitreous fiber. CLSM measurements were *in situ* three-dimensional measurements on fibers in parenchyma.

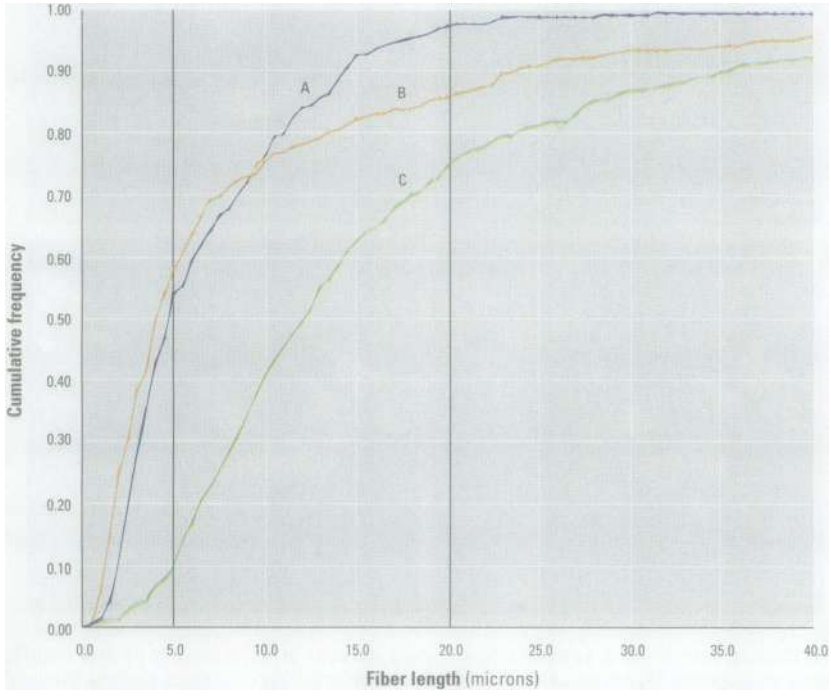

Figure 8. Fiber length cumulative frequency distributions of three types of fibers retained in lung after 13-week exposure as determined *in situ* in three dimensions by confocal laser scanning microscopy. Curve A, man-made vitreous fiber (MMVF)10a; curve B, MMVF33; curve C, long amosite (high dose).

transverse fragmentation). In the present study, the *in situ* CLSM method provides data on fiber length free from any artifacts due to lung destruction. With MMVF10a, *in situ* CLSM produced a postretention FLCFD that overlaid that from ashing/SEM analysis (Figure 6A), suggesting that ashing did not fragment retained MMVF10a fibers significantly. Results from MMVF33 run counter to the breakage-during-ashing hypothesis; the FLCFD from *in situ* CLSM shows a greater proportion of short fibers than that from ashing/SEM. We cannot yet account for this discrepancy. The amosite results, however, were consistent with breakage during ashing; the FLCFD by *in situ* CLSM showed a greater proportion of long fibers than the FLCFD by ashing/SEM, and the numbers of actual fibers/lung determined by SEM were approximately 250% greater than those determined by *in situ* CLSM. However, other differences in the two analytical methodologies may offer a better explanation for the discrepancies in amosite counts.

With only two exceptions (MMVF10a and MMVF33 fibers <5 µm long), fiber burdens estimated by ashing/SEM were greater than those estimated by *in situ* CLSM by factors of 1.4–9.1 (Table 2). The largest difference in counts (ninefold) between the two methods was for amosite fibers <5 µm in length (Table 2). At least two parameters, fiber diameter and fiber distribution throughout the lung, could account for the reduction in the numbers of fibers detected by the *in situ* CLSM method relative to the ashing/SEM method. The images in this study were collected using the CLSM in the reflected light mode and had pixels approximately 0.51 µm on a side. Fibers with diameters ≤0.5 µm may not have reflected enough light to raise the intensity of the image's corresponding pixel(s) above noise level. This could explain the especially large (two- to ninefold) discrepancies between SEM and CLSM counts for amosite, which had smaller mean diameters than the two MMVFs. Additionally, *in situ* CLSM would detect fewer fibers than ashing/SEM if fiber deposition was not homogeneous through the lung. For example, during sparse random imaging of a lung sample by CLSM, it would be relatively rare to encounter fibers clumped in a few dense local concentrations; however, with ashing/SEM analysis, all fibers—whether clumped or isolated—would be equally likely to be counted. Finally, fibers approximately 5 µm long can be phagocytized by alveolar macrophages and cleared to pulmonary lymph nodes, where they may remain for an indefinite period (*25*). Fibers within lymph nodes would have been detected by ashing/SEM, but in the present study no lymph nodes were examined by *in situ* CLSM. This difference between the two methodologies may adequately account for many of the observed discrepancies.

Evaluation of Analysis of Retained Fibers by *in Situ* CLSM

There is room for technical improvements, notably in the increase and calibration of detection sensitivity. Effort also must be made to ensure that fibers are not unduly disturbed during tissue preparation and embedding and that tissue configuration remains reasonably unchanged. In addition, *in situ* analyses are time- and labor-intensive, although advances in speed of image acquisition and subsequent computation continue to ameliorate this situation.

To its credit, *in situ* CLSM analysis brings several advantages to the study of fiber toxicity models. Because retained fibers may be visualized largely undisturbed, their locations relative to cells and surrounding tissue can be studied and

Table 2. Fiber fractions and fiber burdens by length class

	Length class (microns)	Fraction of total fiber number			Fiber burden (number fibers/lung) × 10^{-6}		
		Aerosolized[a] (SEM)	Retained[a] (ashing, SEM)	Retained (CLSM)	Retained[a] (ashing, SEM)	Retained (CLSM)	Burden assay ratio[b]
MMVF10a	Total	–	–	–	24.8	17.6	1.4
	>0–5	0.16	0.38	0.54	9.35	9.47	0.99
	>5–10	0.17	0.38	0.22	9.33	3.92	2.4
	>10–15	0.17	0.14	0.16	3.4	2.88	1.2
	>15–20	0.12	0.06	0.04	1.58	0.82	1.9
	>20	0.38	0.04	0.02	1.09	0.47	2.3
	WHO (>5)	0.84	0.62	0.46	15.4	8.1	1.9
MMVF33	Total	–	–	–	32.8	22.2	1.5
	>0–5	0.33	0.33	0.58	10.8	12.8	0.84
	>5–10	0.14	0.33	0.18	10.8	3.92	2.8
	>10–15	0.2	0.14	0.06	4.74	1.53	3.1
	>15–20	0.14	0.08	0.03	2.78	0.8	3.5
	>20	0.2	0.12	0.14	3.76	3.13	1.2
	WHO (>5)	0.67	0.67	0.42	22	9.35	2.4
Long amosite (high dose)	Total	–	–	–	68.3	19.4	3.5
	>0–5	0.18	0.18	0.09	17	1.87	9.1
	>5–10	0.16	0.16	0.31	23.8	6.05	3.9
	>10–15	0.25	0.25	0.22	11.9	4.24	2.8
	>15–20	0.03	0.03	0.12	6.56	2.41	2.7
	>20	0.38	0.38	0.25	9.04	4.92	1.8
	WHO (>5)	0.82	0.82	0.9	51.3	17.6	2.9

Abbreviations: SEM, scanning electron microscopy; CLSM, confocal laser scanning microscopy; MMVF, man-made vitreous fiber; WHO, World Health Organization. Length distributions of MMVF10a, MMVF33, and long amosite asbestos (high-dosage regimen) fibers, when aerosolized but before inhalation, and fiber burdens and fiber length distributions after 13 weeks exposure, as obtained by ashing/SEM and *in situ* CLSM.

[a]Results from Miiller (*19*).

[b]Values are ratios of fiber burdens [retained (SEM)/retained (CLSM)].

Table 3. Fiber length densities in hamster lungs

Fiber types	$N_{fields\text{-}of\text{-}view}$	$N_{fiber\ profiles}$	L_V[a]
MMVF10a	87	359	30.5
MMVF33	78	267	25.3
Amosite (low dose)	50	135	20.0
Amosite (high dose)	106	1,170	81.6

Abbreviations: L_V, length density of fibers in lung; MMVF, man-made vitreous fiber. Length densities of fibers (four dosage regimens) retained in hamster lungs after 13 weeks exposure, as determined by stereological analysis of optical sections obtained by confocal laser scanning microscopy.

[a]Millimeters per cubic millimeter.

understood. Some progress toward this understanding can be made using the ashing/SEM technique; lungs may be lavaged, and the lavage fluid may be centrifuged so as to pellet the cells (primarily alveolar macrophages) but not the free extracellular fibers, which then remain in the supernatant. Ashing/SEM may be used to examine the fibers in the lavaged lung and the lavage pellet, producing estimates of the fibers that penetrated lung tissue and those which macrophages had engulfed or attempted to engulf. However, this technique is vulnerable to the uncertain nature of lavaging; it is not clear, for instance, whether all fibers in alveolar air spaces would be swept out into the lavage fluid or whether they could remain trapped. Additionally, ashing/SEM still does not provide information on where and how fibers and tissue interact or on whether macrophages ingest fibers successfully. *In situ* CLSM analysis, as shown here, does provide information on these points.

Three-dimensional reconstructions of fibers and tissue can be particularly informative about the modes by which fibers mechanically damage tissue and the mechanisms the organ uses to respond to the insult; in the present study, for example, fibers penetrated septa and airway walls and were partially or entirely engulfed by phagocytes. It would seem possible, also, to use three-dimensional microscopy to study whether fibers and their fragments migrate within tissue or are carried within macrophages, possibly to be cleared from the lung.

References and Notes

1. DeVuyst P, Dumortier P, Swaen GMH, Pairon JC, Brochard P. Respiratory health effects of man-made vitreous (mineral) fibers. Eur Respir J 8:2149–2173 (1995).
2. Hesterberg TW, Chase GR, Axten C, Miiller WC, Musselman RP, Kamstrup O, Hadley J, Morscheidt C, Bernstein DM, Thevenaz P. Biopersistence of synthetic vitreous fibers and amosite asbestos in the rat lung following inhalation. Toxicol Appl Pharmacol 151:262–275 (1998).
3. Davis JMG, Addison J, Bolton RE, Donaldson K, Jones AD, Smith T. The pathogenicity of long versus short fiber samples of amosite asbestos administered to rats by inhalation and intraperitoneal injection. Br J Exp Pathol 67:415–430 (1986).
4. Coin PG, Roggli VL, Brody AR. Persistence of long, thin chrysotile asbestos fibers in the lungs of rats. Environ Health Perspect 102(suppl 5):197–199 (1994).
5. Kelly DP, Williams SJ, Kennedy GL, Lee KP. Recovery and characterization of lung-deposited Kevlar aramid fibers in rats [abstract]. Toxicologist 5:129 (1985).
6. Warheit DB, Hwang HC, Achinko L. Assessments of lung digestion methods for recovery of fibers. Environ Res 54:183–193 (1991).
7. Hesterberg TW, Miiller WC, McConnell EE, Chevalier J, Hadley J, Bernstein DM, Thevenaz P, Anderson R. Chronic inhalation toxicity of size-separated glass fibers in Fischer 344 rats. Fundam Appl Toxicology 20:464–476 (1993).
8. Brody AR, Hill LH, Adkins B, O'Connor RW. Chryostile asbestos inhalation in rats: Deposition pattern and reaction of alveolar epithelium and pulmonary macrophages. Am Rev Respir Dis 123:670–679 (1981).
9. Hesterberg TW, Miiller WC, Musselman RP, Kamstrup O, Hamilton RD, Thevenaz P. Biopersistence of man-made vitreous fibers and crocidolite asbestos in the rat lung following inhalation. Fundam Appl Toxicology 29:267–279 (1996).
10. Hesterberg TW, Axten C, McConnell EE, Oberdörster G, Everitt J, Miiller WC, Chevalier J, Chase GR, Thevenaz P. Chronic inhalation study of fiber glass and amosite asbestos in hamsters: twelve-month preliminary results. Environ Health Perspect 105 (suppl 5):1223–1229 (1997).
11. World Health Organization. Reference Method for Measuring Airborne Man-made Mineral Fibers (MMVF). Environmental Health Report No. 4. Copenhagen, Denmark:World Health Organization, Regional Office for Europe, 1985.
12. McConnell EE, Mast RW, Hesterberg TW, Chevalier J, Kotin P, Bernstein DM, Thevenaz P, Glass LR, Anderson T. Chronic inhalation toxicity of a kaolin-based refractory ceramic fiber (RCF) in Syrian golden hamsters. Inhal Toxicol 7:503–532 (1995).
13. Rogers RA, Oldmixon EH, Brain JD. Enhanced contrast within embedded tissue by lucifer yellow CH—an ideal stain for laser scanning confocal microscopy [abstract]. Mol Biol Cell 3(suppl):185a (1992).
14. Law BD, Bunn WB, Hesterberg TW. Dissolution of natural mineral and man-made vitreous fibers in Karnovsky's and formalin fixatives. Inhal Toxicol 3:309–321 (1991).
15. Oldmixon EH, Brismar H, Lai J, Ekstein B, Rogers RA. Overcoming confocal scanning laser microscopy depth limitations [abstract]. FASEB J 8:A691 (1994).
16. McConnell EE, Kamstrup O, Musselman R, Hesterberg TW, Chevalier J, Miiller WC, Thevenaz P. Chronic inhalation study of size-separated rock and slag wool insulation fibers in Fischer 344/N rats. Inhal Toxicol 6:571–614 (1994).
17. Rogers RA, Antonini JM, Lai J, Ekstein BA, Oldmixon EO, Brain JD. 3-D imaging of natural and artificial respirable size fibers in lung tissue. In: Proceedings in Microscopy and Microanalysis 1995 (Bailey GW, Ellisman MH, Henniger RA, Zaluzec NJ, eds). New York:Jones and Begell Publishing, 1995;1018–1019.
18. Weibel ER. Stereological Methods. Vol. 1: Practical Methods for Biological Morphometry. New York:Academic Press, 1979;143.
19. Miiller WC. Unpublished data.
20. Brody AR, Roe MW. Deposition pattern of inorganic particles at the alveolar level in the lungs of rats and mice. Am Rev Respir Dis 128:724–729 (1983).
21. Wagner JC, Berry G, Skidmore JW, Timbrell V. The effects of the inhalation of asbestos inhalation in rats. Br J Cancer 29:252–269 (1974).
22. Lee KP, Barras CE, Griffith FD, Waritz RS. Pulmonary response to glass fibers by inhalation exposure. Lab Invest 40:123–133 (1979).
23. Lee KP, Kelly DP, Kennedy GL. Pulmonary response to inhaled Kevlar aramid synthetic fibers in rats. Toxicol Appl Pharmacol 71:242–253 (1983).
24. Timbrell V. Deposition and retention of fibres in the human lung. Ann Occup Hyg 26:347–369 (1982).
25. Bernstein, DM, Drew RT, Kuschner M. Experimental approaches for exposure to sized glass fibers. Environ Health Perspect 34:47–57 (1980).